Check for
updates

Turbulence Intensity and Length Scale Effects on Premixed Turbulent Flame Propagation

Shrey Trivedi[1] · R. S. Cant[1]

Abstract

The effects of varying turbulence intensity and turbulence length scale on premixed turbulent flame propagation are investigated using Direct Numerical Simulation (DNS). The DNS dataset contains the results of a set of turbulent flame simulations based on separate and systematic changes in either turbulence intensity or turbulence integral length scale while keeping all other parameters constant. All flames considered are in the thin reaction zones regime. Several aspects of flame behaviour are analysed and compared, either by varying the turbulence intensity at constant integral length scale, or by varying the integral length scale at constant turbulence intensity. The turbulent flame speed is found to increase with increasing turbulence intensity and also with increasing integral length scale. Changes in the turbulent flame speed are generally accounted for by changes in the flame surface area, but some deviation is observed at high values of turbulence intensity. The probability density functions (pdfs) of tangential strain rate and mean flame curvature are found to broaden with increasing turbulence intensity and also with decreasing integral length scale. The response of the correlation between tangential strain rate and mean flame curvature is also investigated. The statistics of displacement speed and its components are analysed, and the findings indicate that changes in response to decreasing integral length scale are broadly similar to those observed for increasing turbulence intensity, although there are some interesting differences. These findings serve to improve current understanding of the role of turbulence length scales in flame propagation.

Keywords Turbulent premixed flames · Turbulence intensity · Turbulence integral length scale

1 Introduction

The response of a premixed flame when subjected to increasingly intense turbulence has been the subject of many different experimental and theoretical studies (Bradley 1992; Driscoll 2008; Peters 1999; Poludnenko and Oran 2011, 2010). Turbulence causes flames to stretch, resulting in an increase of the flame surface area and hence

✉ Shrey Trivedi
   st634@cam.ac.uk

[1] Department of Engineering, University of Cambridge, Cambridge, UK

the burning rate (Damköhler 1940; Pope 1988; Candel and Poinsot 1990; Law 1988). In addition, it has been theorised that small scales of turbulence may enhance the transport due to turbulence and cause further enhancement in the flame speed (Damköhler 1940; Nivarti et al. 2019; Driscoll 2008). A majority of related studies has focused on the variations in turbulence intensity (Driscoll 2008; Lipatnikov and Chomiak 2002), including Direct Numerical Simulation (DNS) studies which have been applied to investigate the effect of increasing the turbulence intensity u' while holding all other parameters constant as far as possible (Nivarti and Cant 2017).

There have been fewer studies which have produced information about the effect on the flame of varying the turbulence integral length scale l_0 (Peters 1999; Lipatnikov and Chomiak 1999; Song et al. 2021). Several experimental investigations dealing with variations in ℓ_0 have been discussed in Sect. 3.3.2 in Ref. (Lipatnikov and Chomiak 2002). This is harder to achieve in DNS, due to the need to resolve the full range of turbulence length scales from the integral scale down to the Kolmogorov scale η. Therefore, given the high computational cost, the scope for variation of the integral length scale l_0 is necessarily limited. Nevertheless, fundamental study of the effect of length scales is important in order to explore the combustion physics, to define the constraints on flamelet-based modelling (Driscoll et al. 2020; Skiba et al. 2017, 2021; Hawkes and Chen 2006) and to suggest model improvements. Recent papers have analysed the variations in flame speed with ℓ_0 both experimentally (Kim et al. 2020; Mohammadnejad et al. 2021) and using DNS (Yu and Lipatnikov 2017a, b; Kulkarni and Bisetti 2021a; Kulkarni et al. 2021; Kulkarni and Bisetti 2021b; Varma et al. 2021).

The dependence of flame speed on the turbulence Reynolds number was investigated experimentally (Smith and Gouldin 1979; Shy et al. 2015) and showed any increase in flame speed with an increasing turbulent Reynolds number, consistent with the previous predictions (Damköhler 1940; Peters 1999). Recent analysis based on DNS of turbulent slot jet flames (Attili et al. 2021; Luca et al. 2019) investigated flames at nearly constant Karlovitz number (Ka) but with variations in Reynolds number (Re). The key finding of this work was that thickening of the inner reaction layer occurs as Re increases, causing the flame speed to increase faster than the flame area as Re increases (Attili et al. 2021). Furthermore, the statistics of flame stretch for this dataset (Luca et al. 2019) indicated that tangential strain rate and mean flame curvature normalised by the Kolmogorov length η were found to have a weak dependence on Re.

The present study aims to investigate the response of a turbulent premixed flame to variations in u' and l_0, treating each of these quantities separately as an independent variable while holding all the other variables constant. Unlike the previous analyses (Attili et al. 2021; Luca et al. 2019), the Komogorov scale and hence the Karlovitz number changes across the dataset.

The rest of the paper is organised as follows. Section 2 presents the relevant theory to outline and define the flame properties of interest. A matrix of test cases is described in Sect. 3 covering a range of both of the independent variables of interest. Section 4 presents the results for the flame properties including flame speed and flame area, statistics of tangential strain rate and mean flame curvature, and statistics of displacement speed and its components. The effects of varying u' at constant l_0 are compared with previous findings (Nivarti and Cant 2017), while results illustrating the effects of varying l_0 at constant u' are also presented and discussed.

2 Theory

The increase in flame surface area A_T due to the action of turbulence (Law 1988; Pope 1988) and the subsequent increase in the turbulent flame speed s_T has been studied extensively both experimentally (Driscoll 2008) and computationally (Chen et al. 1999; Poludnenko and Oran 2011; Nivarti and Cant 2017), and is governed by the expression

$$\frac{s_T}{s_L} \sim \frac{A_T}{A_L} \Rightarrow \frac{s_T}{s_L} = \frac{A_T}{A_L} I_0 \tag{1}$$

where I_0 is the stretch factor (Driscoll 2008; Bray and Cant 1991). Note that the above relationship is valid under the Klimov-Williams limit (Klimov 1963; Williams 1985), i.e. when all turbulence length scales are larger than δ_L. In the above expression, the turbulent flame speed s_T can be evaluated using the integral

$$s_T = -\frac{1}{\rho_R Y_{FR} A_0} \int_V \dot{\omega}_F dV \tag{2}$$

where ρ_R and Y_{FR} are the unburnt mixture density and fuel mass fraction respectively and A_0 is the cross sectional area of the domain. It is convenient to introduce a reaction progress variable c (based for example on normalised fuel mass fraction) which rises montonically from zero in fresh reactants to unity in fully-burned products. The relation between flame area and flame surface density is stated as

$$A_T = \int_{-\infty}^{\infty} \Sigma dV \tag{3}$$

The flame surface density Σ is important in premixed combustion modelling (Pope 1988; Peters 1999; Candel and Poinsot 1990; Cant et al. 1990), and can be defined as the expected value of the flame surface area per unit volume for an isosurface at $c = c^*$, i.e.

$$\Sigma = \overline{\Sigma'} \tag{4}$$

where the "fine–grained" flame surface density Σ' can be defined by using the gradient of progress variable (Boger et al. 1998) according to

$$\Sigma' = \frac{\delta A}{\delta V} = |\nabla c| \delta(c - c^*) \tag{5}$$

The balance equation for Σ takes the form Pope (1988), Candel and Poinsot (1990)

$$\frac{\partial \Sigma}{\partial t} + \frac{\partial}{\partial x_i}(u_i + S_d n_i)\Sigma = \dot{S}\Sigma \tag{6}$$

where the flame normal vector n_i is given by

$$n_i = -\frac{\nabla c}{|\nabla c|}, \tag{7}$$

and the displacement speed S_d of the flame is obtained using the expression

$$\rho S_d \sigma = \dot{\omega} + \frac{\partial}{\partial x_k}\left(\rho D \frac{\partial c}{\partial x_k}\right) \tag{8}$$

where σ is the generalised FSD (Boger et al. 1998) defined as $\sigma = \overline{|\nabla c|}$. The flame stretch rate $\dot{S}$ is defined as the fractional rate of increase of flame area

$$\dot{S} = \frac{1}{A}\frac{dA}{dt} = a_t + 2S_d\kappa \tag{9}$$

where a_t is the rate of hydrodynamic strain tangential to the flame and κ is the mean curvature of the flame. An expression for a_t can be stated as

$$a_t = (\delta_{ij} - n_i n_j)\frac{\partial u_i}{\partial x_j} \tag{10}$$

where δ_{ij} is the Kronecker delta, and the mean curvature κ is defined as

$$\kappa = \frac{1}{2}\frac{\partial n_i}{\partial x_i} \tag{11}$$

Flame stretch can have significant effects on the internal structure of the flame (Law 1988). These effects can be accounted for using the stretch factor I_0 (Bray and Cant 1991; Driscoll 2008), defined as the ratio of local instantaneous propagation speed s_L^* to the unstrained laminar flame speed s_L:

$$I_0 = \frac{s_L^*}{s_L} \tag{12}$$

The quantity I_0 has been found to be ~ 1 for thermo-diffusively neutral mixtures, i.e. $Le = 1$, but the value of I_0 has been found to deviate from unity for non-unity Lewis numbers (Hawkes and Chen 2006; Bradley 1992; Lipatnikov and Chomiak 2002) or for very high values of Karlovitz number (Driscoll 2008). Moreover, thickening of the flame can enhance the flame speed over and above that estimated by change in flame area alone (Attili et al. 2021; Nivarti et al. 2019) leading to values of I_0 greater than unity.

3 DNS Dataset for the Current Study

The simulations were carried out using the well-established in-house DNS code SENGA2 (Jenkins and Cant 1999; Cant 2012). This code solves the Navier–Stokes momentum equations in their compressible form, augmented by conservation equations for mass and energy and by balance equations for the relevant chemical species mass fractions. The spatial discretisation scheme uses 10th order explicit centred finite differences, reducing smoothly to 4th order one-sided differences at non-periodic boundaries. Time-stepping is effected using a 4th-order low–storage explicit Runge–Kutta algorithm with adaptive step-size control (Kennedy and Carpenter 2003). The code is fully parallelised using a domain decomposition technique. Boundary conditions are imposed using the Navier–Stokes Characteristic Boundary Condition (NSCBC) formalism (Poinsot and Lele 1992).

For the purposes of the present study, the chemistry is treated using a single-step Arrhenius formulation tuned to replicate the flame propagation speed s_L of a stoichiometric methane—air flame, i.e. 39 cm/s, and also to capture the corresponding thermal flame thickness δ_L given as $\delta_L = (T^b - T^u)/(dT/dx)_{max}$, where T^b and T^u are the temperature of the burnt and unburnt gas respectively. The density ratio of the burned to unburned gases is ~ 0.13.

The Lewis number of the reacting species is set to unity. It is acknowledged that single—step chemistry may not capture all the details of the flame—turbulence interaction, and this will be investigated in future work using a more detailed chemical reaction mechanism.

The computational domain consists of a cuboid with periodic boundary conditions in the spanwise y and z directions. The streamwise x direction has NSCBC outflow boundary conditions on opposite faces. The thermochemical pressure is set to 1 bar and the reactant temperature is set to 300 K. The dataset created for analysis is based on a pair of statistically planar flames facing each other with fresh reactants between them. The flames are simulated in a cuboidal domain of cross section 5 mm × 5 mm. Turbulence of the required intensity and integral length scale is generated using a spectral algorithm (Orszag 1972) initialised with the Bachelor–Townsend spectrum (Batchelor and Townsend 1948) and is imposed on the domain. The turbulence in the unburned reactants is forced linearly (Lundgren 2003) in order to counteract the process of decay and hence to maintain the required properties. A known shortcoming of Lundgren's method (Lundgren 2003) is that the turbulent length scale changes over time until it reaches a steady value (Klein et al. 2017; Rosales and Meneveau 2005). Klein et al. (2017) attempted to fix this issue by making the forcing term proportional to a high pass filtered value of velocity. However, no such correction has been applied in this work and it is likely that the associated length scales of turbulence change in time. In future, this issue will be addressed..

Within the dataset, both turbulence intensity u' and integral length scale ℓ_0 are varied systematically. For values of $u'/s_L = 10$, 20 and 30, simulations are carried out with integral length scales corresponding to $\ell_0/\delta_L = 5.0$, $\ell_0/\delta_L = 2.0$ and $\ell_0/\delta_L = 1.25$. For $u'/s_L = 40$ only the case of $\ell_0/\delta_L = 2.0$ is simulated. The mesh spacing Δx is varied in each case to match the Kolmogorov scale η and the simulation time was kept at 6 eddy turnover times, i.e. $t/\tau = 6$ for all cases. A summary of the parameters for each simulation is provided in Table 1.

The separation between the flames is varied for each individual case such that the flames do not collide even at the end of the run. The forcing region was kept between the two flames and of the forced region varied between cases since each case had different separation between flames. The width of the forced region was chosen such that it does not interact with the flames during the run time. Figure 1 shows results from the cases with three different ℓ_0 values for $u'/s_L = 10$. For the highest ℓ_0 value (Fig. 1a), the large scale wrinkling requires larger separation between the two flames whereas for the smaller ℓ_0 values (Fig. 1b and c) a smaller separation is sufficient to keep the two flames from interacting.

Table 1 Main parameters of the different cases in the dataset

	ℓ_0/δ_L	Ka	Da	Re	η (μm)	τ_η (μs)	Δx (μm)
$u'/s_L = 10$	5.0	14.14	0.5	50	39.27	11.03	41.66
	2.0	22.36	0.2	20	24.85	6.97	26.04
	1.25	28.28	0.125	12.5	20.33	5.51	20.833
$u'/s_L = 20$	5.0	40.0	0.25	100	28.76	3.9	26.04
	2.0	63.25	0.1	40	18.19	2.46	14.38
	1.25	80.0	0.0625	25	14.38	1.95	13.02
$u'/s_L = 30$	5.0	73.5	0.166	150	23.48	2.12	22.72
	2.0	116.2	0.0667	60	14.85	1.34	13.02
	1.25	147.0	0.0417	37.5	11.90	1.06	11.90
$u'/s_L = 40$	2.0	179	0.05	80	12.86	0.87	11.90

(a) $\ell_0/\delta_L = 5.0$

(b) $\ell_0/\delta_L = 2.0$
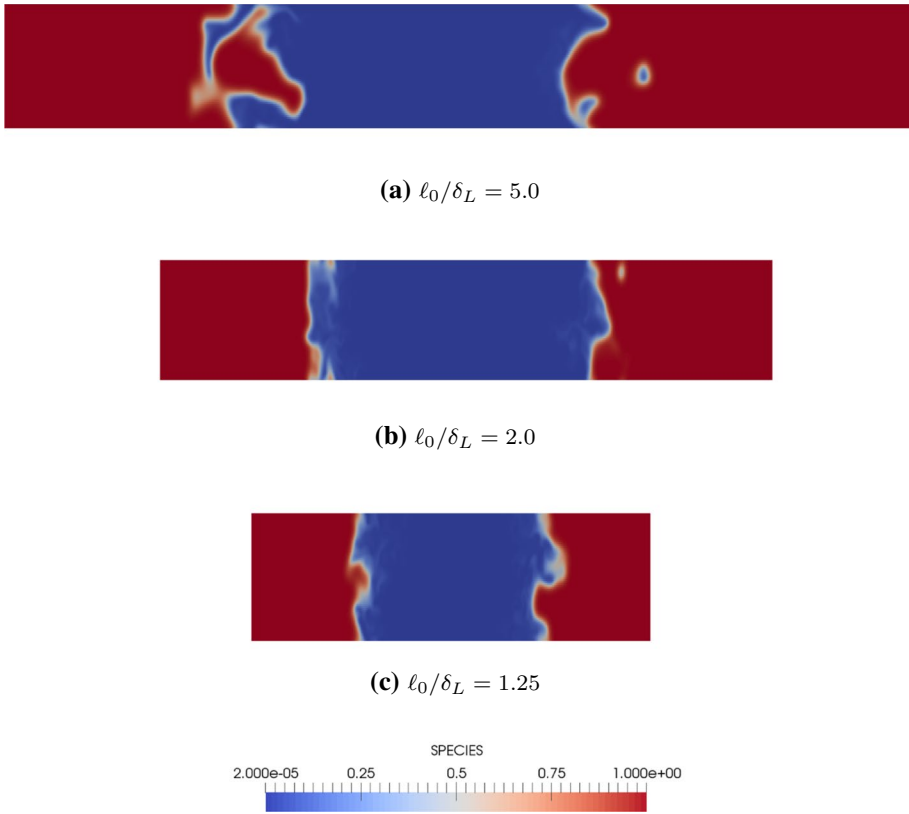

(c) $\ell_0/\delta_L = 1.25$

Fig. 1 Two dimensional slices of the 3-D snapshots of product mass fraction for cases $\ell_0/\delta_L = 5.0$, $\ell_0/\delta_L = 2.0$ and $\ell_0/\delta_L = 1.25$ (top to bottom) for fixed $u'/s_L = 10$. The separation between the flames is adjusted to keep them from interacting

The dataset can be used to analyse the effects of integral length scale ℓ_0 while keeping the turbulence intensity u' fixed. Alternatively, a fixed value of ℓ_0 can be chosen and the variation in u' can be studied. Note that the Kolmogorov scale η also decreases as ℓ_0 decreases and/or u' increases. The data points corresponding to the dataset are presented on a Borghi diagram as shown in Fig. 2. All the cases are either in, or very close to, the thin reaction zones regime. It has been noted that broken reaction zones are not observed even well beyond Ka=100 (Aspden et al. 2019; Song et al. 2021), which was also found to be true for all of the present cases. In all cases, the turbulent flame approached a statistically stationary state, albeit with considerable fluctuations of s_T about its mean value, as observed in other work (Poludnenko and Oran 2011; Lipatnikov et al. 2015).

4 Results

In this section, the flame properties are presented as functions of the systematic variations in both u' and ℓ_0. The results for increasing u' at a fixed value of ℓ_0 are found to be consistent with those from the literature (Nivarti and Cant 2017; Lipatnikov and Chomiak 2002). The

Fig. 2 Representation of the current DNS dataset on a Borghi diagram
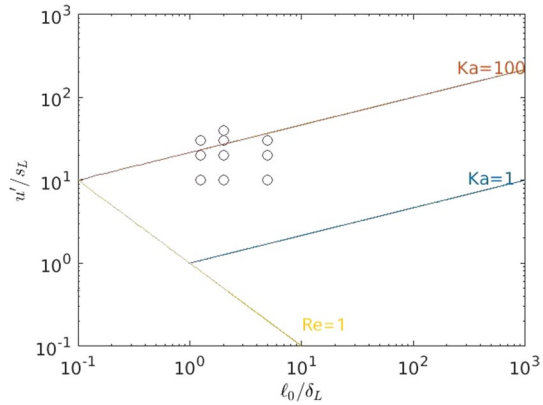
results for varying ℓ_0 at constant u' are presented for analysis, and comparisons are drawn between the known trends for increasing u' versus those observed for varying ℓ_0.

Turbulent flame speed and flame area are analysed first, followed by the probability density functions (pdfs) of mean curvature, tangential strain rate and displacement speed. Subsequently, the correlations between strain, curvature, displacement speed and its components are evaluated and presented.

4.1 Turbulent Flame Speed

The turbulent flame speed s_T and flame area A_T (for the isosurface at $c = 0.8$) are evaluated using Eqs. 2 and 3 respectively and are normalised with the unstrained laminar flame speed s_L and the domain cross—sectional area A_L for the full dataset. The turbulent flame speed s_T is plotted against u' (also normalised with s_L) in Fig. 3 with different lines representing different values of ℓ_0. It can be seen that s_T increases with u' for all values of ℓ_0. Furthermore, the values of s_T are higher for larger values of ℓ_0, i.e.

$$s_{T,\ell_0/\delta_L=5.0} > s_{T,\ell_0/\delta_L=2.0} > s_{T,\ell_0/\delta_L=1.25}$$

This behaviour is consistent with previous simulation results for increasing u' (Nivarti and Cant 2017; Lipatnikov and Chomiak 2002) as well as with previous analyses (Peters 1999; Lipatnikov and Chomiak 1999). Note that the values of s_T/s_L obtained here are similar to

Fig. 3 Turbulent flame speed s_T/s_L plotted against turbulence intensity u'/s_L for three different values of integral length scale ℓ_0/δ_L equal to 5.0, 2.0 and 1.25
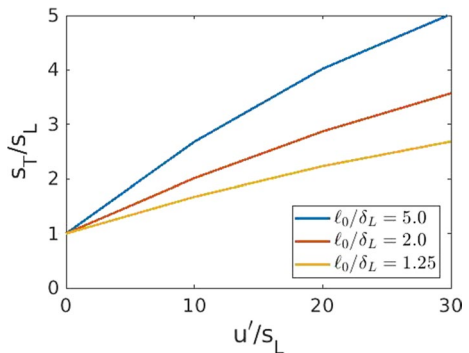
those obtained in the constant density flows (for example in Sabelnikov et al. (2019)) as well as in variable density flow (Nivarti and Cant 2017), consistent with the discussion in Lipatnikov et al. (2018).

Values of s_T/s_L are also presented in Table 2 along with the corresponding values of A_T/A_L and the ratio $I_0 = (s_T/s_L)/(A_T/A_L)$ (see Eq. 1). There are several important observations to be made from this table. First, the area ratio A_T/A_L follows the same trend as s_T/s_L in that values corresponding to $\ell_0/\delta_L = 5.0$ are higher than those corresponding to $\ell_0/\delta_L = 2.0$ and $\ell_0/\delta_L = 1.25$ for each u' value. It can be seen that s_T/s_L (and also A_T/A_L) differs by around a factor of two between $\ell_0/\delta_L = 5.0$ and $\ell_0/\delta_L = 1.25$. This indicates that the principal factor affecting the turbulent flame speed is the increase of flame surface area, due to either higher turbulence intensity or larger turbulence integral length scale causing increased large-scale flame wrinkling.

Following Refs. (Kulkarni and Bisetti 2021a; Chaudhuri et al. 2012), a power—law fit for the dependence of S_T on Reynolds number in the form $S_T \sim \mathrm{Re}^n$ was found to yield an exponent $n \sim 0.4$ which is similar but lower than the findings of Chaudhuri et al. (2012) ($n \sim 0.5$) and Kulkarni et al. (2021) ($n \sim 0.56$). This could be a result of the differences in flow configuration, fuel type or the fact that the Reynolds numbers used here are lower than in these studies. This merits further investigation using a DNS dataset covering a greater range of Reynolds number than is accessible in the present work.

At the same time, the value of I_0 becomes greater than unity as u' increases for the two cases with larger ℓ_0, and especially for the case with the largest value of $\ell_0/\delta_L = 5.0$. Likewise, the values of I_0 also increase slightly as u' increases for any fixed value of ℓ_0. This indicates that factors other than the flame area, such as changes to the internal structure of the local flame sheet due to strain and curvature may affect the observed increase in the turbulent flame speed. However, the values of I_0 remain very close to unity for all the cases and hence require further investigation. An increase in I_0 with Reynolds number was reported by Attili et al. (2021) caused by the thickening of the inner flame layer. In the present study, the values of I_0 for any given u' do not change significantly as the values of ℓ_0 change.

For each value of u', it can be seen from Table 2 (4th column) that the decrease in A_T/A_L as ℓ_0 decreases is monotonic but is not linear. The ratio $(A_T/A_L)/(\ell_0/\delta_L)$ is presented in the rightmost column of the table. This ratio is lowest for the cases with $\ell_0/\delta_L = 5.0$ and increases for the cases with smaller length scales. This provides an indication that an

Table 2 Turbulent flame speed s_T and flame surface area A_T (evaluated at $c = 0.8$) normalised by unstrained laminar flame speed s_L and domain cross section area A_L respectively for all cases

u'/u_L	ℓ_0/δ_L	s_T/s_L	A_T/A_L	I_0	$(A_T/A_L)/(\ell_0/\delta_L)$
10	5.0	3.237	3.296	0.982	0.659
	2.0	2.287	2.299	0.995	1.149
	1.25	1.758	1.776	0.989	1.421
20	5.0	3.805	3.830	0.993	0.766
	2.0	2.753	2.704	1.018	1.352
	1.25	2.256	2.194	1.028	1.755
30	5.0	5.023	4.907	1.024	0.981
	2.0	3.571	3.398	1.051	1.699
	1.25	2.685	2.619	1.024	2.095
40	2.0	4.628	4.160	1.112	2.080

Values of I_0 and the ratio $(A_T/A_L)/(\ell_0/\delta_L)$ are also presented

increasing amount of small-scale turbulence plays a role in increasing the flame surface area, and is more efficient in doing so at lower values of ℓ_0.

The flame surface density Σ conditioned on progress variable c is presented in Fig. 4. Figure 4a shows the plots for fixed $\ell_0/\delta_L = 2.0$ and increasing u' while Fig. 4b represents those for a fixed u'/S_L ($= 20$) but decreasing ℓ_0. The conditional value of Σ decreases as u' increases. This is because even though the flame area increases, the volume corresponding to the wrinkled flame surface also increases. It is interesting to note that the same trend of decreasing Σ is observed also for decreasing ℓ_0 at fixed u', and indeed the similarity between Figs. 4a and b is striking. Note that there are no significant changes in the profiles of Σ for $c > 0.6$ and hence the changes in Σ are mostly restricted to the preheat zone, consistent with the previous findings (Nivarti and Cant 2017).

Fig. 4 Flame surface density Σ conditioned on progress variable c for **a** varying u' at fixed $\ell_0 = 2.0\delta_L$ and **b** varying ℓ_0 at fixed $u' = 20\ s_L$
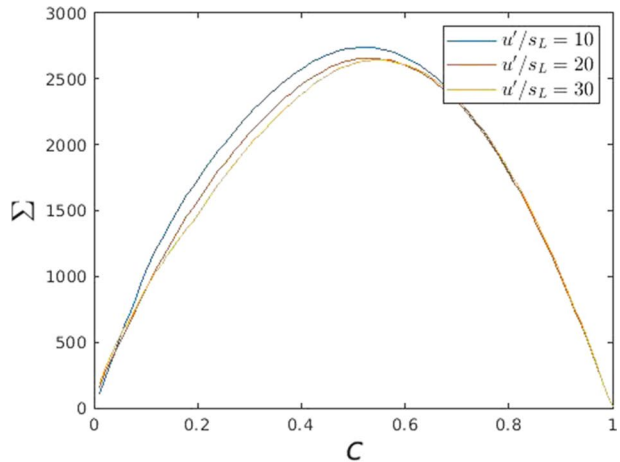

**(a)** Flame surface density for different u' at a fixed $\ell_0 = 2.0\delta_L$.
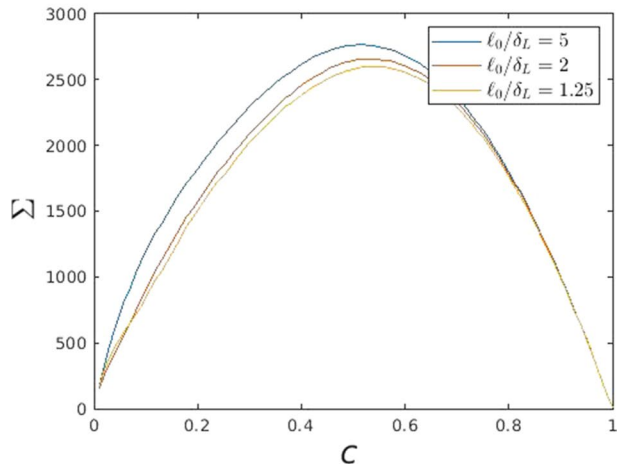
(b) Flame surface density for different ℓ_0 at a fixed $u' = 20\ s_L$.
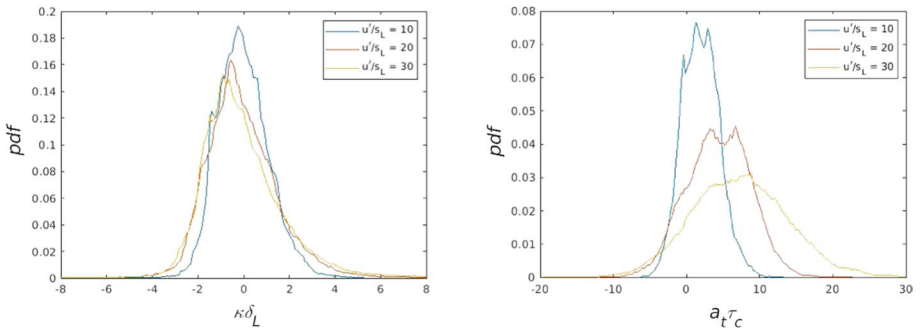
4.2 Curvature and Strain Rate

In this subsection, the pdfs of mean curvature κ and tangential strain rate a_t are plotted for different values of u' and ℓ_0. These pdfs are analysed for the isosurface corresponding to $c = 0.8$. First, the pdfs of curvature and tangential strain rate are presented in Fig. 5 for varying u' at fixed values of ℓ_0. The curvature pdfs are shown in the left column while the tangential strain rate pdfs are shown in the right column. The pdfs
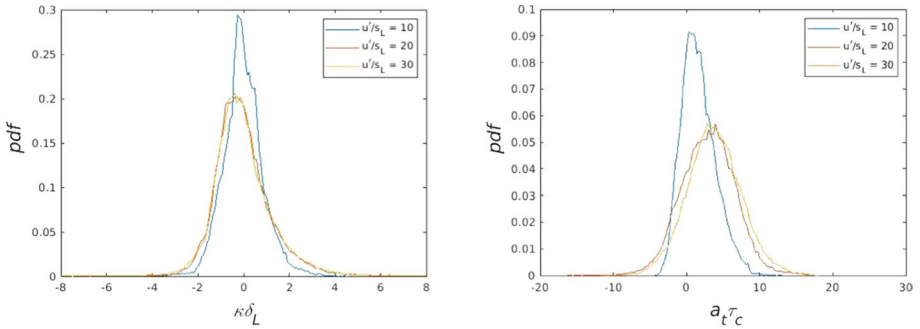
(a) Pdfs of mean curvature (left) and tangential strain rate (right) at $\ell_0/\delta_L = 5.0$.
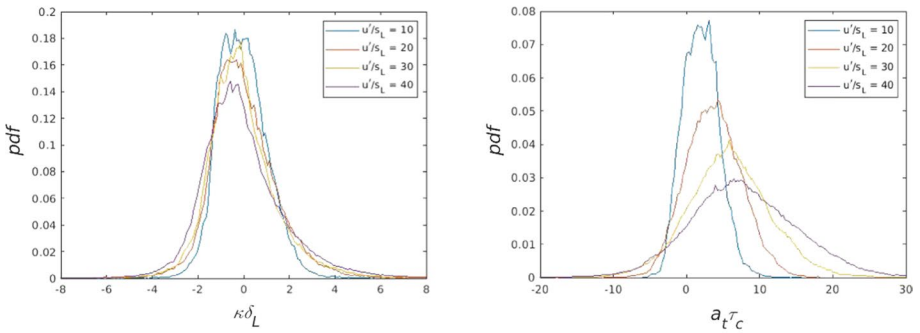
(b) Pdfs of mean curvature (left) and tangential strain rate (right) at $\ell_0/\delta_L = 2.0$.

(c) Pdfs of mean curvature (left) and tangential strain rate (right) at $\ell_0/\delta_L = 1.25$.

Fig. 5 Pdfs of mean curvature (left column) and strain rate (right column) for different values of u'/s_L and fixed $\ell_0/\delta_L = 5.0$ (top row), 2.0 (middle row) and 1.25 (bottom row)

corresponding to $\ell_0/\delta_L = 5.0$, 2.0 and 1.25 are shown in the top, middle and bottom row respectively.

Looking at the mean curvature pdfs (Fig. 5, left column), as u' is increased from 10 (red line) to 20 (blue line) to 30 (yellow line), the pdfs become wider and their peak value decreases, and this is true for all values of ℓ_0/δ_L. On physical grounds, the increase in the width of the mean curvature pdf is expected since at higher u' the eddies have more energy available to wrinkle the flame surface. Furthermore, at higher u' there is an addition of Kolmogorov—scale eddies since $\eta_{u'/s_l=10} > \ldots > \eta_{u'/s_L=30}$. These additional scales lie in the range $\eta_{u'/s_l=10} > l > \eta_{u'/s_L=20}$ for the $u'/s_L = 20$ case and likewise for $u'/s_L = 30$ case. These additional smaller scales result in higher values of κ ($\sim 1/R$) and hence broader pdfs. The behaviour of these pdfs is consistent with the results in a previous analysis by Nivarti and Cant (2017) and for the experimental results for V-flames (Kheirkhah and Gülder 2013). It is also interesting to note that the height and width of the mean curvature pdfs for $u'/s_L = 20$ and 30 are similar to each other, suggesting that there is some tendency towards saturation of flame curvature at higher turbulence intensity.

For the tangential strain rate pdfs (Fig. 5, right column) the height of the peaks decreases and their width increases as u'/s_L increases, for all values of ℓ_0/δ_L. The effect is most pronounced for the highest u' cases for which the pdf becomes significantly broader which was also observed from the experimental results of spherically expanding flames (Liu et al. 2021). The peak of the pdf for all cases is observed at a positive value of a_t, and this value becomes more positive as u'/s_L increases which is consistent with previous DNS findings (Nivarti and Cant 2017). Again, these effects result from greater energy within the eddies at higher u'/s_L. The additional smaller scales strain the flame surfaces more effectively due to their higher velocity gradients. Note that the flame thickness δ_L and flame time $\tau_c (= \delta_L/L)$ are used to normalise κ and a_t respectively. This is done so that the normalisation still shows the differences between the results across the dataset, since δ_L and τ_c are constant for all cases presented here. It is expected that other scales are better suited for such normalisation, and to justify the above phenomenological explanations. These will be explored in future work.

Results showing the variation in the pdfs of mean curvature κ and tangential strain rate a_t with changes in ℓ_0/δ_L for fixed values of u'/s_L are presented in Fig. 6. As in Fig. 5 the mean curvature pdfs are shown in the left column while the tangential strain rate pdfs are shown in the right column. The pdfs corresponding to $\ell_0/\delta_L = 5.0$, 2.0 and 1.25 are represented by blue, red and yellow coloured lines respectively (see legend). The values of u'/s_L are 10 (top row), 20 (middle row) and 30 (bottom row).

In each plot, the available mean kinetic energy of the turbulence is the same and hence changes in the pdf are due only to the different length scales of turbulence. It can be seen by comparison with Fig. 5 that the trends observed for decreasing ℓ_0/δ_L are similar to those for increasing u'/s_L. The pdf of κ (left column) for all values of u' has the greatest peak value but smallest overall width for the highest value of $\ell_0/\delta_L = 5.0$ (blue line). The pdfs become lower and wider as the value of ℓ_0/δ_L decreases to 2.0 (red line) and to 1.25 (yellow line).

As the value of ℓ_0/δ_L decreases, the corresponding Kolmogorov length scale η also decreases, i.e. $\eta_{\ell_0/\delta_L=5.0} > \ldots > \eta_{\ell_0/\delta_L=1.25}$. This introduces an additional range of smaller length scales between $\eta_{\ell_0/\delta_L} = 5.0 > l > \eta_{\ell_0/\delta_L} = 2.0$ for the $\ell_0/\delta_L = 2.0$ case. These additional small scales for each case correspond to higher κ ($\sim 1/R$) and result in higher probability of high curvature events as ℓ_0 decreases. Hence, the width of the mean curvature pdfs increases. Likewise, since the cases at lower ℓ_0 contain fewer large scale eddies, the probability of low curvature events decreases, and thus the peak height of
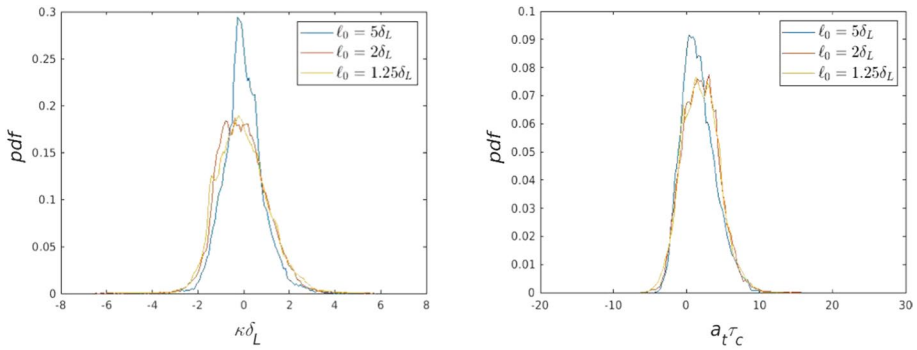
(a) Pdf of mean curvature (left) and tangential strain rate (right) at $u'/s_L = 10$.
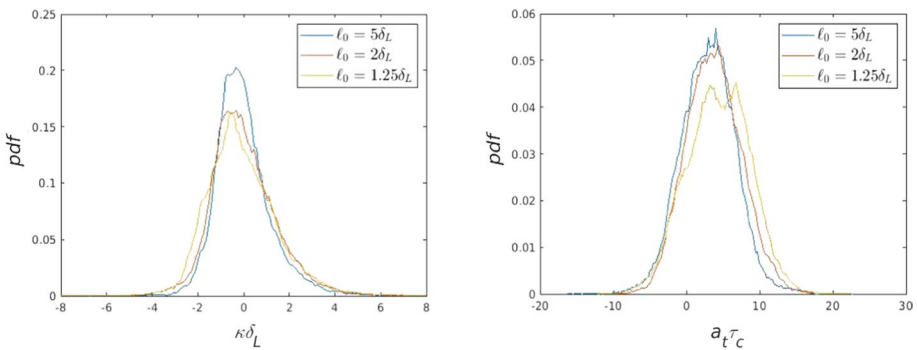
(b) Pdfs of mean curvature (left) and tangential strain rate (right) at $u'/s_L = 20$.
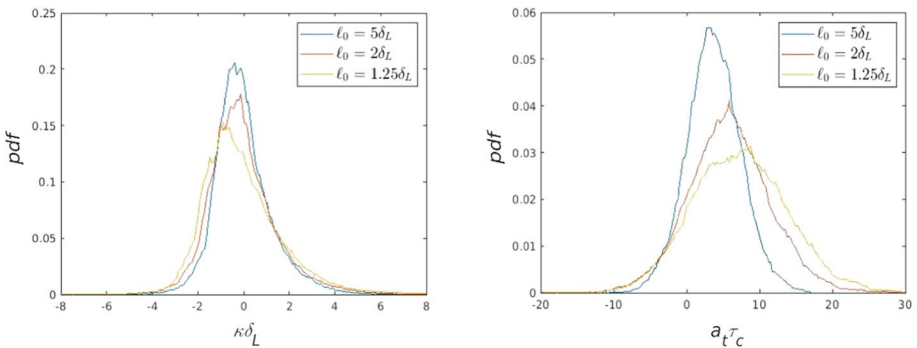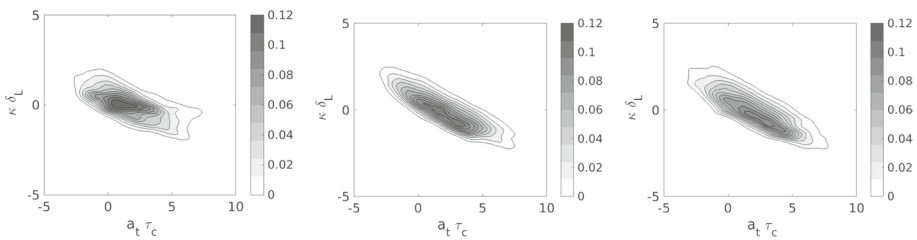

(c) Pdfs of mean curvature (left) and tangential strain rate (right) at $u'/s_L = 30$.

Fig. 6 Pdfs of mean curvature (left column) and strain rate (right column) for different values of ℓ_0/δ_L and fixed $u'/s_L = 10$ (top row), 20 (middle row) and 30 (bottom row)

the pdf decreases. The height and width of the pdfs for $\ell_0/\delta_L = 2.0$ and $\ell_0/\delta_L = 1.25$ remains roughly the same, again suggesting a tendency towards saturation in curvature for values of ℓ_0/δ_L less than about 2.0. Note that the peak of the κ pdfs occurs close to zero curvature for all values of ℓ_0.

Turning to the changes in the pdfs of tangential strain rate for different values of ℓ_0/δ_L (Fig. 6, right column), for all values of u' the peak value of each pdf is again the highest for the largest integral length scale, i.e. $\ell_0/\delta_L = 5.0$. The pdfs become lower and their width increases as ℓ_0/δ_L decreases, but the mean tangential strain rate remains positive for all cases. Also, the value of a_t at the peak becomes increasingly positive with decreasing ℓ_0/δ_L. Again, the smaller values of Kolmogorov scale η for smaller values of ℓ_0/δ_L result in greater positive straining of the flame due to their large velocity gradients. Once again, on comparing Figs. 5 and 6 it can be seen that for both κ and a_t there is considerable similarity in the changes observed in the pdfs in response to either increasing u'/s_L or decreasing ℓ_0/δ_L. As before, proper scaling will be needed in future for greater clarity on the above explanations.

The correlation between mean curvature κ and tangential strain rate a_t can be observed from the joint pdfs of these quantities in the form of iso-probability curves shown in Fig. 7. The subfigures on the top row show the correlation between κ and a_t for $u'/s_L = 10$, the middle row shows $u'/s_L = 20$ and bottom row shows $u'/s_L = 30$. The value of ℓ_0/δ_L

(a) Joint pdfs of mean curvature κ and tangential strain rate a_t at $u'/s_L = 10$ and $\ell_0/\delta_L =$ 5.0, 2.5 and 1.25 from left to right respectively.
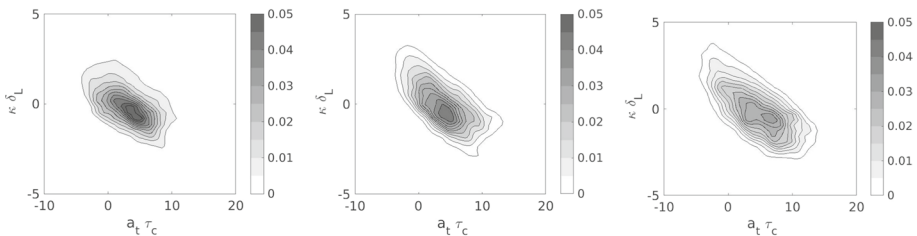
(b) Joint pdfs of mean curvature κ and tangential strain rate a_t at $u'/s_L = 20$ and $\ell_0/\delta_L =$ 5.0, 2.5 and 1.25 from left to right respectively.
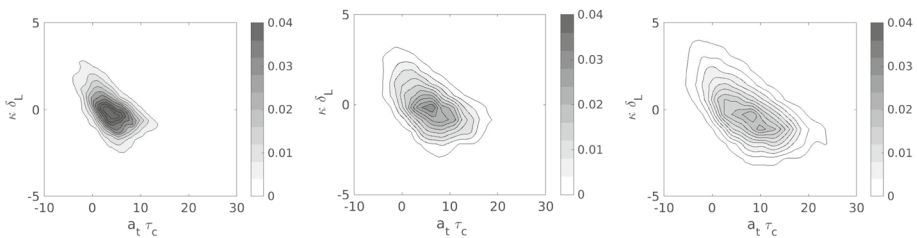
(c) Joint pdfs of mean curvature κ and tangential strain rate a_t at $u'/s_L = 30$ and $\ell_0/\delta_L =$ 5.0, 2.5 and 1.25 from left to right respectively.

Fig. 7 joint pdfs of mean curvature and tangential strain rate for different values of ℓ_0/δ_L (left to right) and for different values of u'/s_L (top to bottom)

decreases from 5.0 to 2.0 and then to 1.25 in the left, middle and right subfigures respectively in each row.

In all cases, a negative correlation between κ and a_t is observed. Similar plots have been presented in the past for increasing u' (and fixed ℓ_0) (Nivarti and Cant 2019), and these showed a negative correlation between κ and a_t which weakened as u' was increased. This is a consequence of greater wrinkling of the flame due to higher energy in all scales of turbulent eddies. The current results also show the same trend with u' at fixed ℓ_0 (Fig. 7, top to bottom in any column). By contrast, the strength of the κ–a_t correlation tends to increase slightly at each fixed value of u' as ℓ_0/δ_L is decreased. This is consistent with the broadening of the strain rate pdf (see Fig 6 right column) at fixed u', which indicates that the available kinetic energy (for a fixed u') is spread over a greater range of length scales giving a better match with the length scales of flame curvature.

### 4.3 Displacement Speed Statistics

It is interesting to consider the pdf of the displacement speed S_d and its dependence on flame stretch quantities. The pdfs of S_d are presented in Fig. 8a for different values of u'/s_L at fixed $\ell_0/\delta_L = 2.0$, and in Fig. 8b for different values of ℓ_0/δ_L at fixed $u'/s_L = 20$.

It can be seen that the displacement speed pdfs exhibit similar trends to those observed for the mean curvature and tangential strain rate pdfs. For increasing values of u'/s_L at fixed ℓ_0/δ_L, the pdfs become shorter and wider, and the same pattern is observed for decreasing ℓ_0/δ_L at fixed u'/s_L. In all cases, the mean value of S_d was found to be $\sim \rho s_L/\rho_R$ where ρ_R is the reactant density.

The relatively strong correlation between S_d and flame stretch, i.e. both strain and curvature, ensures that the pdfs of S_d (Fig. 8) also become shorter and broader in a similar manner to the of κ and a_t pdfs with either increasing u' (Fig. 5) or decreasing ℓ_0 (Fig. 6).

Joint pdfs of displacement speed S_d and mean curvature κ in the form of iso-probability curves are shown in Fig. 9a (top row) while those for displacement speed and tangential strain rate a_t are shown in Fig. 9a (bottom row). For both rows, the value of $\ell_0/\delta_L = 2.0$ is fixed while u'/s_L increases from 10 (left) to 20 (middle) to 30 (right). A distinct negative correlation can be seen between S_d and κ (top row). The negative correlation is stronger for positive curvature than for negative curvature, as observed in previous studies (Chakraborty and Cant 2005b; Nivarti and Cant 2019) and explained in terms of the combined effects of both curvature and strain rate on the different components of displacements speed. As u' increases, the strength of the correlation between S_d and κ remains broadly unchanged. There is a positive correlation between S_d and a_t (bottom row), and this is consistent with the negative correlation observed between κ and a_t (see Fig. 7). As u' increases the underlying positive correlation between S_d and a_t weakens somewhat, and there is a tendency to favour S_d/s_L close to unity at low mean curvature for a broad range of strain rates, again as previously observed (Chakraborty and Cant 2005a; Nivarti and Cant 2019).

Further joint pdfs of S_d and κ are shown in Fig. 9b (top row) while joint pdfs of S_d and a_t are shown in Fig. 9b (bottom row), but this time the value of $u'/s_L = 20$ is held fixed while ℓ_0/δ_L is varied from 5.0 (left) to 2.0 (middle) to 1.25 (right). Comparison of Fig. 9a and b shows that the trends for the S_d–κ joint pdfs with decreasing ℓ_0 are similar to those observed for increasing u'. This is less apparent for the S_d-a_t joint pdfs (bottom row). Here the tendency for S_d/s_L to cluster close to unity weakens as ℓ_0 decreases, due to the lower probability of finding low mean curvatures (see Fig. 5 left column).
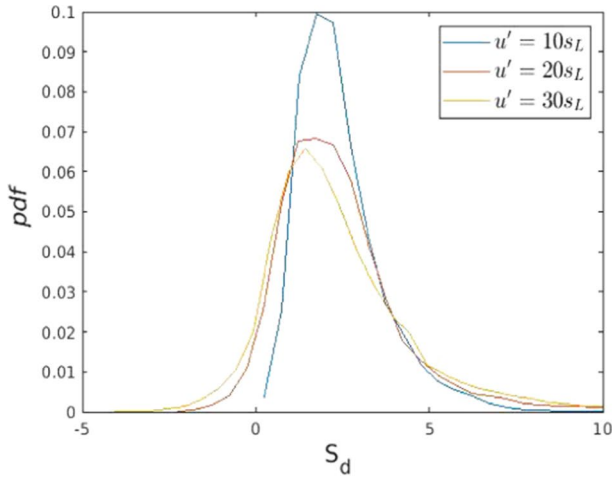
**(a)** Pdf of displacement speed S_d for a range of values of u'/s_L at fixed $\ell_0/\delta_L = 2.0$.
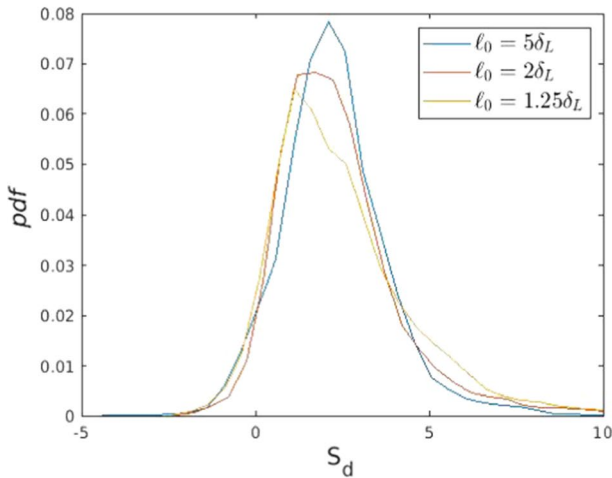
(b) Pdf of displacement speed S_d for a range of values of ℓ_0/δ_L at fixed $u'/s_L = 20$.

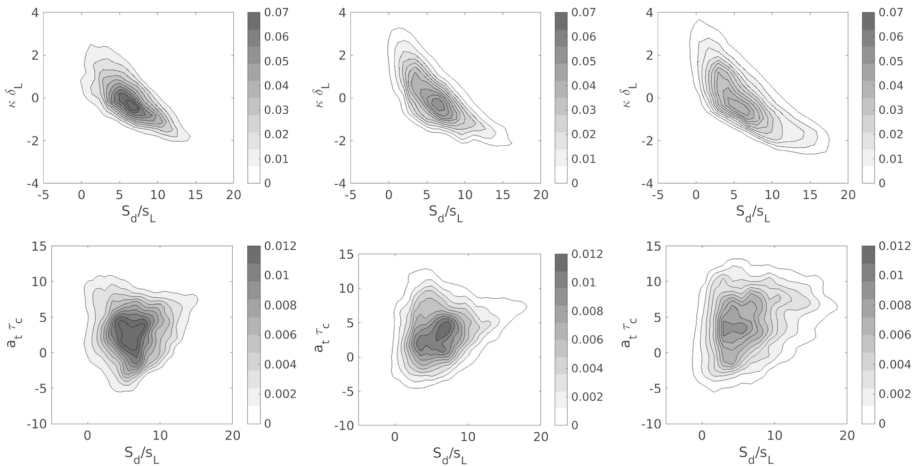**Fig. 8** Probability density functions of displacement speed S_d for **a** different values of u' at fixed $\ell_0/\delta_L = 2.0$ and **b** different values of ℓ_0/δ_L at fixed $u'/s_L = 20$

The correlation coefficients corresponding to the joint pdfs presented above are summarised in Tables 3 and 4. First, correlation coefficients for increasing u' at a fixed $\ell_0/\delta_L = 2.0$ are shown in Table 3. Consistent with Fig. 7, the correlation coefficient for the κ-a_t correlation becomes less negative, i.e. the correlation becomes weaker as the turbulence intensity increases and the same is true for the S_d-a_t correlation, while the S_d-κ correlation coefficient does not change much. Similar results were found for all values of ℓ_0/δ_L.

The corresponding correlation coefficients for a fixed value of u'/s_L at different values of ℓ_0/δ_L are shown in Table 4. The S_d-a_t correlation coefficient is positive and increases
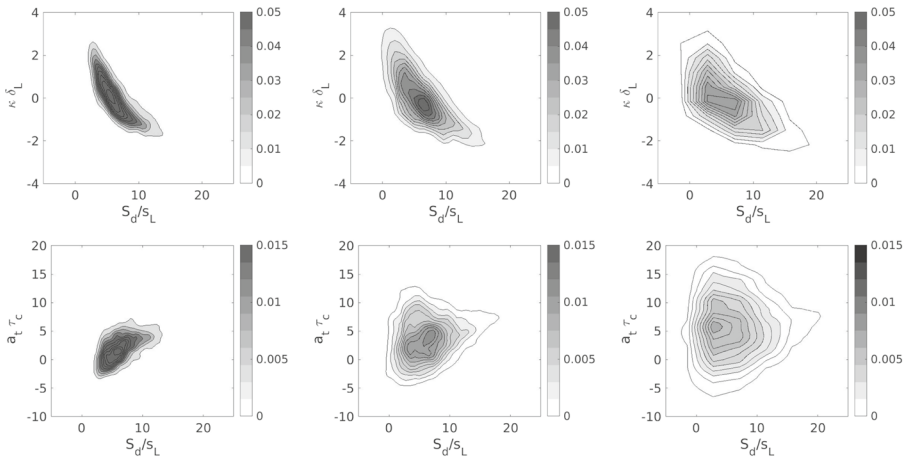
(a) Joint pdfs of displacement speed S_d with κ (top row) and a_t (bottom row) for values of $u'/s_L = 10$ (left), 20 (middle) and 30 (right) at fixed $\ell_0/\delta_L = 2.0$.

(b) Joint pdfs of displacement speed S_d with κ and a_t for a values of $\ell_0/\delta_L = 5.0$ (left), 2.0 (middle) and 1.25 (right) at fixed $u'/s_L = 20$.

Fig. 9 Joint pdfs of displacement speed S_d with κ and a_t for **a** different values of u' at fixed $\ell_0/\delta_L = 2.0$ and **b** different values of ℓ_0/δ_L at fixed $u'/s_L = 20$

Table 3 Correlation coefficients over a range of u'/s_L at fixed $\ell_0/\delta_L = 2.0$		u'/s_L	$\kappa - a_t$	$S_d - a_t$	$S_d - \kappa$
	$\ell_0/\delta_L = 2.0$	10	-0.732	0.514	-0.454
		20	-0.553	0.390	-0.525
		30	-0.450	0.241	-0.530

slightly with decreasing ℓ_0/δ_L. The S_d–κ correlation coefficient, however, is negative and broadly constant for these cases.

Table 4 Correlation coefficients over a range of ℓ_0/δ_L at fixed $u'/s_L = 20$

		ℓ_0/δ_L	$\kappa - a_t$	$S_d - a_t$	$S_d - \kappa$
$u'/s_L = 20$		5.0	− 0.476	0.271	− 0.489
		2.0	− 0.553	0.390	− 0.525
		1.25	− 0.565	0.379	− 0.552

The different components of displacement speed, i.e. the reaction component S_r, normal diffusion component S_n and tangential diffusion component S_t are defined by

$$S_r = \frac{\dot{\omega}}{\rho\sigma}; \quad S_n = -\frac{n_k}{\rho\sigma}\frac{\partial}{\partial x_k}(\rho D\sigma); \quad S_t = -2D\kappa \qquad (13)$$

The joint pdfs for the reaction and normal diffusion components of S_d with κ and a_t are presented in Fig. 10 for fixed ℓ_0 and varying u'. The first row shows the joint pdfs of the normal diffusion component S_n with κ while the second row shows the reaction component S_r with κ. Similarly, the third row shows S_n with a_t while the fourth row shows S_r with a_t. The left, middle and right columns show the joint pdfs for u'/s_L = 10, 20 and 30 respectively. Joint pdfs are not shown for the tangential component S_t since this component is deterministically related to κ (see eqn. 13).
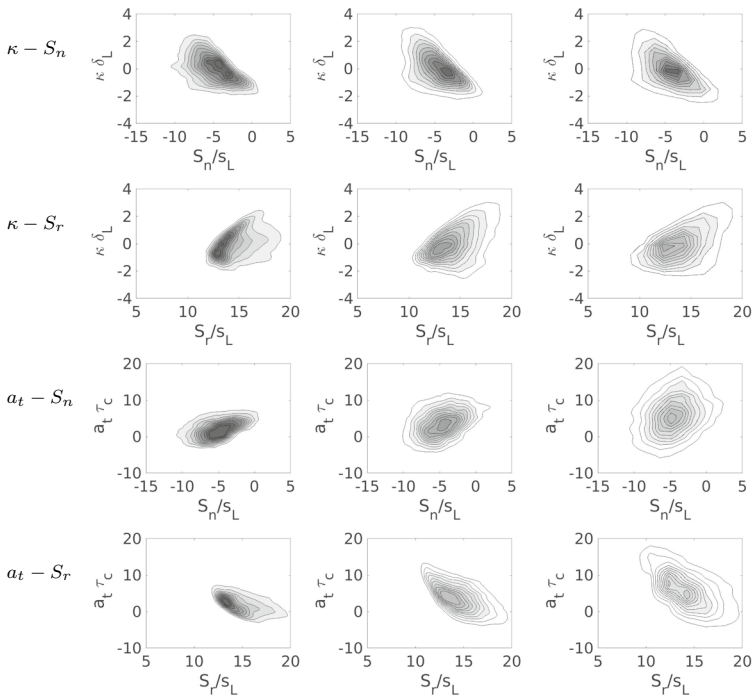

Fig. 10 Joint pdfs of different components of the displacement speed with κ and a_t for different values of u'/s_L at fixed $\ell_0/\delta_L = 2.0$

Table 5 Correlation coefficients for the correlations between the reaction (S_r), normal diffusion (S_n) and tangential diffusion (S_t) components of displacement speed with mean curvature κ and tangential strain rate a_t over a range of u'/s_L at fixed $\ell_0/\delta_L = 2.0$

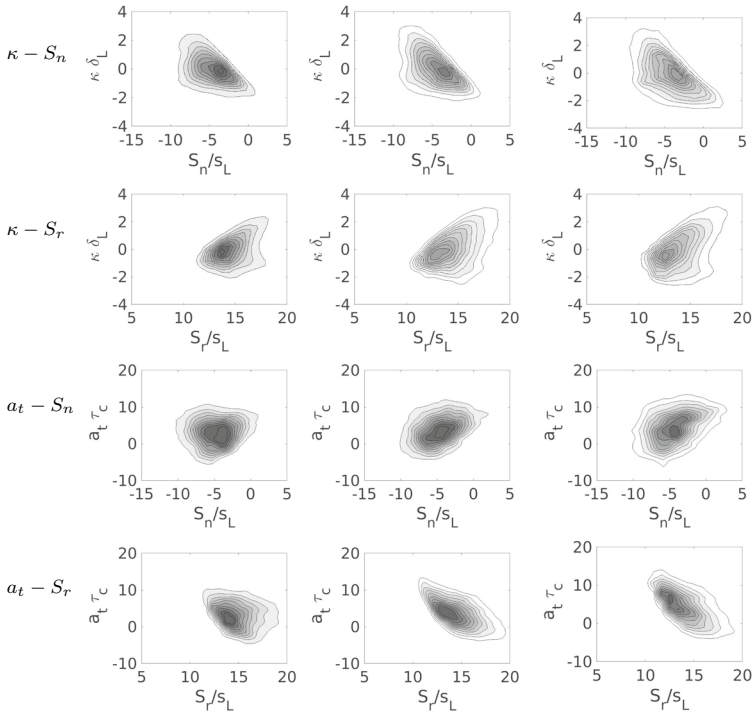|	u'/s_l	$S_r - a_t$	$S_n - a_t$	$S_t - a_t$	$S_r - \kappa$	$S_n - \kappa$	$S_t - \kappa$
$\ell_0/\delta_L = 2.0$	10	0.190	0.031	0.732	0.067	− 0.297	− 1.0
	20	0.194	− 0.012	0.553	0.110	− 0.428	− 1.0
	30	0.166	− 0.039	0.450	0.092	− 0.484	− 1.0

Fig. 11 Joint pdfs of different components of the displacement speed with κ and a_t for different values of ℓ_0/δ_L at fixed $u'/s_L = 20$

The relevant correlation coefficients are presented in Table 5 for a fixed value of $\ell_0/\delta_L = 2.0$ and increasing u'/s_L. The correlation between S_t and a_t (fourth column) is of the same value but opposite sign to that between κ and a_t (see Table 4) since S_t is directly proportional to negative κ. This also results in a correlation coefficient between S_t and κ equal to negative unity (right column). The normal component of displacement speed S_n shows a very weak correlation with a_t (third column) but a negative correlation with κ (second column from the right). On the other hand, the reaction component S_r shows a positive correlation with a_t (second column) and a weak correlation with κ (third column from the right). These results are consistent with the findings of several previous studies (Chakraborty and Cant 2005a, b; Nivarti and Cant 2019).

Corresponding joint pdfs for the reaction and normal diffusion components of S_d with κ and a_t are presented in Fig. 11 for fixed $u'/s_L = 20$ and varying ℓ_0/δ_L. Again the first row

shows normal diffusion component S_n with κ while the second row S_r with κ. The third row shows S_n with a_t while the fourth row shows S_r with a_t. The left, middle and right columns show the joint pdfs for $\ell_0/\delta_L = 5.0, 2.0$ and 1.25 respectively. Comparison of Figs. 11 with 10 indicates a strong similarity between the joint pdfs for S_n and S_r with κ (top two rows in each Figure), as well as similar trends for the plots of S_n and S_r with a_t (bottom two rows in each Figure).

Again, the correlation between S_t and a_t (fourth column) is the same in value but opposite in sign to that of κ and a_t (see Fig. 5). There is a perfect negative correlation between S_t and κ (right column), i.e. the correlation coefficient is equal to negative unity. As in the previous cases, S_n has a weak correlation with a_t (third column) while S_r has a positive correlation with a_t (second column). The correlation between S_n and κ is negative (second column from the right) while the correlation between S_r and κ is weakly positive (third column from the right).

For the displacement speed components, the trends with decreasing ℓ_0 at fixed u' are broadly similar to those observed for increasing u' at fixed ℓ_0. The correlation between S_n and a_t remains weak for all cases, and this is true also for the correlation between S_r and κ. The negative correlation between S_n and κ becomes stronger for variations in either u' or ℓ_0. The correlation between S_r and a_t is positive and weakens with increasing u', whereas for decreasing ℓ_0 the positive correlation strengthens slightly, consistent with the trends observed for the correlation between κ and a_t. The correlation between S_t and a_t in all cases simply reflects the correlation between κ and a_t and the deterministic dependence of S_t on κ.

5 Conclusions

A set of Direct Numerical Simulations has been carried out in which the integral length scale ℓ_0/δ_L as well as the turbulence intensity u'/s_L is varied in a systematic manner while keeping all other parameters constant. A twin flame configuration has been used in which the separation between the flames is kept sufficiently large so that the flames do not collide. Linear forcing of the turbulence has been applied between the two flames so that the turbulence does not decay rapidly as the flames propagate towards each other.

The turbulent flame speed s_T and flame area A_T have been evaluated for all the cases. The turbulent flame speed is found to be greatest for the highest value of ℓ_0 at a fixed value of u', consistent with previous predictions (Peters 1999; Damköhler 1940) and DNS data (Nivarti et al. 2019). The ratio of s_T/s_L to A_T/A_L is found to be close to unity but increases

Table 6 Correlation coefficients for the correlations between the reaction (S_r), normal diffusion (S_n) and tangential diffusion (S_t) components of displacement speed with mean curvature κ and tangential strain rate a_t over a range of ℓ_0/δ_L at fixed $u'/s_L = 20$

	ℓ_0/δ_L	$S_r - a_t$	$S_n - a_t$	$S_t - a_t$	$S_r - \kappa$	$S_n - \kappa$	$S_t - \kappa$
$u'/s_L = 20$	5.0	0.186	− 0.124	0.476	0.135	− 0.382	− 1.0
	2.0	0.194	− 0.012	0.553	0.110	− 0.428	− 1.0
	1.25	0.200	0.028	0.565	0.063	− 0.451	− 1.0

slightly as u'/s_L increases for fixed values of the length scale ratio ℓ_0/δ_L. The flame surface density Σ has been evaluated for variations in both u' and ℓ_0. Changes observed for decreasing values of ℓ_0 at fixed u' are found to be remarkably similar to those observed for increasing values of u' at fixed ℓ_0.

The probability density functions (pdfs) of the mean flame curvature and tangential strain rate have been analysed, again with the focus on varying ℓ_0/δ_L for fixed u'/s_L. It has been found that as ℓ_0 decreases, the pdfs of both mean curvature and tangential strain rate become broader and flatter. The peak of the curvature pdfs shifts to a slightly more negative value whereas that of the strain rate shifts to a more positive value.

Analysis the displacement speed S_d indicates similar trends. The pdfs of S_d become broader and flatter with decreasing ℓ_0 at fixed u', just as they do with increasing u' at fixed ℓ_0. Correlations between displacement speed and mean curvature, as well as those between displacement speed and tangential strain rate, have been investigated using joint pdfs and correlation coefficients. The corresponding correlations for the reaction, normal diffusion and tangential diffusion components of displacement speed have been investigated also. The results for increasing u' at fixed ℓ_0 are consistent with previous observations, and the variations observed for decreasing ℓ_0 at fixed u' are found to be broadly similar.

Future work will focus on extending the range of values of ℓ_0/δ_L that can be explored. This will require larger computational domains and correspondingly larger computational resources. Proper scaling for the quantities presented in this paper and their dependence on the Reynolds number will be explored. It will also be necessary also to extend the study to incorporate any effects of chemistry. More detailed investigation of the physics of small-scale turbulence-flame interactions will be carried out, and the implications for modelling will be explored.

Declarations

References

Aspden, A.J., Day, M.S., Bell, J.B.: Towards the distributed burning regime in turbulent premixed flames. J. Fluid Mech. **871**, 1–21 (2019). https://doi.org/10.1017/jfm.2019.316

Attili, A., Luca, S., Denker, D., Bisetti, F., Pitsch, H.: Turbulent flame speed and reaction layer thickening in premixed jet flames at constant Karlovitz and increasing Reynolds numbers. Proc. Combust. Inst. **38**(2), 2939–2947 (2021). https://doi.org/10.1016/j.proci.2020.06.210

Batchelor, G.K., Townsend, A.A.: Decay of turbulence in the final period. Proc. R. Soc. Lond. **A194**, 527–543 (1948)

Boger, M., Veynante, D., Boughanem, H., Trouve, A.: Direct numerical simulation analysis of flame surface density concept for large eddy simulation of turbulent premixed combustion. In: twenty seventh symposium (international) on combustion **27**, 917–925 (1998)

Bradley, D.: How fast can we burn?. In: twenty-fourth symposium (international) on combustion, the combustion institute pp. 247–262 (1992)

Bray, K.N.C., Cant, R.S.: Some applications of Kolmogorov's turbulence research in the field of combustion. Proc. R. Soc. A **434**, 217–240 (1991)

Candel, S.M., Poinsot, T.J.: Flame stretch and the balance equation for the flame area. Combust. Sci. Technol. **70**, 1–15 (1990)

Cant, R.S.: Senga2 user guide. Technical Report CUED-THERMO (2012)

Cant, R.S., Pope, S.B., Bray, K.N.C.: Modelling of flamelet surface-to-volume ratio in turbulent premixed combustion. In: Twenty-third symposium (international) on combustion, the combustion institute pp. 809–815 (1990)

Chakraborty, N., Cant, R.S.: Effects of strain rate and curvature on surface density function transport in turbulent premixed flames in the thin reaction zones regime. Phys. Fluids **17**(6), 065108 (2005). https://doi.org/10.1063/1.1923047

Chakraborty, N., Cant, R.S.: Influence of Lewis number on curvature effects in turbulent premixed flame propagation in the thin reaction zones regime. Phys. Fluids **17**(10), 105105 (2005). https://doi.org/10.1063/1.2084231

Chaudhuri, S., Wu, F., Zhu, D., Law, C.K.: Flame speed and self-similar propagation of expanding turbulent premixed flames. Phys. Rev. Lett. **108**, 044503 (2012). https://doi.org/10.1103/PhysRevLett.108.044503

Chen, J.H., Echekki, T., Kollman, W.: The mechanism of two-dimensional pocket formation in lean premixed methane-air flames with implications to turbulent combustion. Combust. Flame **116**, 15–48 (1999)

Damköhler, G.: Der einfluss der turbulenz auf die flammengeschwindigkeit in gasgemischen. Z. Elektrochem. Angew. Phys. Chem. **46**(11), 601–626 (1940). https://doi.org/10.1002/bbpc.19400461102

Driscoll, J.F.: Turbulent premixed combustion: flamelet structure and its effect on turbulent burning velocities. Progress Energy Combust. Sci. **34**, 91–134 (2008)

Driscoll, J.F., Chen, J.H., Skiba, A.W., Carter, C.D., Hawkes, E.R., Wang, H.: Premixed flames subjected to extreme turbulence: some questions and recent answers. Progress Energy Combust. Sci. **76**, 100802 (2020). https://doi.org/10.1016/j.pecs.2019.100802

Hawkes, E.R., Chen, J.H.: Comparison of direct numerical simulation of lean premixed methane-air flames with strained laminar flame calculations. Combust. Flame **144**, 112–125 (2006)

Jenkins, K.W., Cant, R.S.: Direct Numerical Simulation of Turbulent Flame Kernels. In: Knight, D., Sakell, L. (eds.) Recent Advances in DNS and LES, pp. 191–202. Springer, Dordrecht (1999)

Kennedy, C.A., Carpenter, M.H.: Additive Runge-Kutta schemes for convection-diffusion-reaction equations. Appl. Numerical Math. **11**(1), 139–181 (2003). https://doi.org/10.1016/S0168-9274(02)00138-1

Kheirkhah, S., Gülder, L.: Turbulent premixed combustion in v-shaped flames: characteristics of flame front. Phys. Fluids **25**(5), 055107 (2013). https://doi.org/10.1063/1.4807073

Kim, J., Satija, A., Lucht, R.P., Gore, J.P.: Effects of turbulent flow regime on perforated plate stabilized piloted lean premixed flames. Combust. Flame **211**, 158–172 (2020). https://doi.org/10.1016/j.combustflame.2019.09.027

Klein, M., Chakraborty, N., Ketterl, S.: A comparison of strategies for direct numerical simulation of turbulence chemistry interaction in generic planar turbulent premixed flames. Flow Turbul. Combust. **99**, 955–971 (2017)

Klimov, A.M.: Laminar flame in turbulent flow. Prikladnoy Mekhaniki i Tekhnicheskoy Fiziki Zhurnal (English translation AD-A200 241 Foreign Technology Division. Air Force Syst. Command **3**, 49–58 (1963)

Kulkarni, T., Bisetti, F.: Analysis of the development of the flame brush in turbulent premixed spherical flames. Combusti. Flame **234**, 111640 (2021). https://doi.org/10.1016/j.combustflame.2021.111640

Kulkarni, T., Bisetti, F.: Surface morphology and inner fractal cutoff scale of spherical turbulent premixed flames in decaying isotropic turbulence. Proc. Combust. Inst. **38**(2), 2861–2868 (2021). https://doi.org/10.1016/j.proci.2020.06.117

Kulkarni, T., Buttay, R., Kasbaoui, M.H., Attili, A., Bisetti, F.: Reynolds number scaling of burning rates in spherical turbulent premixed flames. J. Fluid Mech. **906**, 25–89 (2021). https://doi.org/10.1017/jfm.2020.784

Law, C.K.: Dynamics of stretched flames. Proc. Combust. Inst. **22**, 1381–1402 (1988)

Lipatnikov, A., Chomiak, J.: Effects of turbulence length scale on flame speed: a modelling study. In: Rodi, W., Laurence, D. (eds.) Engineering Turbulence Modelling and Experiments, vol. 4, pp. 841–850. Elsevier Science Ltd, Oxford (1999). https://doi.org/10.1016/B978-008043328-8/50081-3

Lipatnikov, A., Chomiak, J.: Turbulent flame speed and thickness: phenomenology, evaluation, and application in multi-dimensional simulations. Progress Energy Combust. Sci. **28**, 1–74 (2002)

Lipatnikov, A.N., Chomiak, J., Sabelnikov, V.A., Nishiki, S., Hasegawa, T.: Unburned mixture fingers in premixed turbulent flames. Proc. Combust. Inst. **35**(2), 1401–1408 (2015). https://doi.org/10.1016/j.proci.2014.06.081

Lipatnikov, A.N., Chomiak, J., Sabelnikov, V.A., Nishiki, S., Hasegawa, T.: A DNS study of the physical mechanisms associated with density ratio influence on turbulent burning velocity in premixed flames. Combust. Theory Model. **22**(1), 131–155 (2018). https://doi.org/10.1080/13647830.2017.1390265

Liu, Z., Unni, V.R., Chaudhuri, S., Law, C.K., Saha, A.: Local statistics of laminar expanding flames subjected to Darrieus–Landau instability. Proc. Combust. Inst. **38**(2), 1993–2000 (2021). https://doi.org/10.1016/j.proci.2020.06.118

Luca, S., Attili, A., Lo Schiavo, E., Creta, F.: On the statistics of flame stretch in turbulent premixed jet flames in the thin reaction zone regime at varying Reynolds number. Proc. Combust. Inst. **37**(2), 2451–2459 (2019). https://doi.org/10.1016/j.proci.2018.06.194

Lundgren, T.S.: Linearly Forced Isotropic Turbulence. Annual Research Briefs, pp. 461–473. CTR, Stanford (2003)

Mohammadnejad, S., An, Q., Vena, P., Yun, S., Kheirkhah, S.: Contributions of flame thickening and extinctions to a heat release rate marker of intensely turbulent premixed hydrogen-enriched methane-air flames. Combust. Flame **231**, 111481 (2021). https://doi.org/10.1016/j.combustflame.2021.111481

Nivarti, G.V., Cant, R.S.: Direct numerical simulation of the bending effect in turbulent premixed flames. Proc. Combust. Inst. **36**, 1903–1910 (2017)

Nivarti, G.V., Cant, R.S.: Stretch rate and displacement speed correlations for Increasingly–Turbulent premixed flames. Flow Turbul. Combust. **102**, 957–971 (2019). https://doi.org/10.1007/s10494-018-9990-7

Nivarti, G.V., Cant, R.S., Hochgreb, S.: Reconciling turbulent burning velocity with flame surface area in small-scale turbulence. J. Fluid Mech. **858**, 25–87 (2019)

Orszag, S.A.: Numerical methods for the simulation of turbulence. Phys. Fluids Suppl. **2**, 250–257 (1972)

Peters, N.: The turbulent burning velocity for large-scale and small-scale turbulence. J. Fluid Mech. **384**, 107–132 (1999)

Poinsot, T., Lele, S.: Boundary conditions for direct simulations of compressible viscous flows. J. Comput. Phys. **101**, 104–129 (1992)

Poludnenko, A.Y., Oran, E.S.: The interaction of high-speed turbulence with flames: global properties and internal flame structure. Combust. Flame **157**, 995–1011 (2010)

Poludnenko, A.Y., Oran, E.S.: The interaction of high-speed turbulence with flames: turbulent flame speed. Combust. Flame **158**, 301–326 (2011)

Pope, S.B.: The evolution of surfaces in turbulence. Int. J. Eng. Sci. **26**, 445–469 (1988)

Rosales, C., Meneveau, C.: Linear forcing in numerical simulations of isotropic turbulence: physical space implementations and convergence properties. Phys. Fluids **17**, 095106 (2005)

Sabelnikov, V.A., Yu, R., Lipatnikov, A.N.: Thin reaction zones in constant-density turbulent flows at low Damköhler numbers: theory and simulations. Phys. Fluids **31**(5), 055104 (2019). https://doi.org/10.1063/1.5090192

Shy, S., Liu, C., Lin, J., Chen, L., Lipatnikov, A., Yang, S.: Correlations of high-pressure lean methane and syngas turbulent burning velocities: effects of turbulent Reynolds, Damköhler, and Karlovitz numbers. Proc. Combust. Inst. **35**(2), 1509–1516 (2015). https://doi.org/10.1016/j.proci.2014.07.026

Skiba, A.W., Carter, C.D., Hammack, S.D., Driscoll, J.F.: High-fidelity flame-front wrinkling measurements derived from fractal analysis of turbulent premixed flames with large Reynolds numbers. Proc. Combust. Insti. **38**(2), 2809–2816 (2021). https://doi.org/10.1016/j.proci.2020.06.041

Skiba, A.W., Wabel, T.M., Carter, C.D., Hammack, S.D., Temme, J.E., Lee, T., Driscoll, J.F.: Reaction layer visualization: a comparison of two plif techniques and advantages of khz-imaging. Proc. Combust. Inst. **36**, 4593–4601 (2017)

Smith, K.O., Gouldin, F.C.: Turbulence effects on flame speed and flame structure. AIAA J. **17**(11), 1243–1250 (1979). https://doi.org/10.2514/3.61305

Song, W., Hernández Pérez, F.E., Tingas, E., Im, H.G.: Statistics of local and global flame speed and structure for highly turbulent H_2/air premixed flames. Combust. Flame **232**, 111523 (2021). https://doi.org/10.1016/j.combustflame.2021.111523

Varma, A.R., Ahmed, U., Klein, M., Chakraborty, N.: Effects of turbulent length scale on the bending effect of turbulent burning velocity in premixed turbulent combustion. Combust. Flame **233**, 111569 (2021). https://doi.org/10.1016/j.combustflame.2021.111569

Williams, F.A.: Combustion Theory. Westview Press, Boulder (1985)

Yu, R., Lipatnikov, A.N.: Direct numerical simulation study of statistically stationary propagation of a reaction wave in homogeneous turbulence. Phys. Rev. E **95**, 063101 (2017). https://doi.org/10.1103/PhysRevE.95.063101

Yu, R., Lipatnikov, A.N.: DNS study of dependence of bulk consumption velocity in a constant-density reacting flow on turbulence and mixture characteristics. Phys. Fluids **29**(6), 065116 (2017). https://doi.org/10.1063/1.4990836